Benefit of the Potential Future Hyperspectral Satellite Sensor (BIODIVERSITY) for Improving the Determination of Water Column and Seabed Features in Coastal Zones

Audrey Minghelli, Sayoob Vadakke-Chanat, Malik Chami, Mireille Guillaume, and Marion Peirache

***Abstract*—Most of the studies dealing with seabed mapping from hyperspectral images have been carried out using airborne data although hyperspectral satellite sensors have already been or are planned to be launched for the near future (hyperspectral imager for the coastal ocean (HICO) environmental mapping and analysis program (ENMAP) or BIODIVERSITY). The objective of this study is to evaluate the benefit of a BIODIVERSITY-like sensor to determine the bio-optical properties of the water column, namely the Chlorophyll-a concentration, the suspended particulate matter (SPM) concentration, the absorption coefficient of the colored dissolved organic matter (CDOM), the bathymetry and the composition of the seabed, according to its spatial resolution and spectral resolution and its signal to noise ratio. For this purpose, radiative transfer simulations are analyzed together with remote sensing hyperspectral airborne data acquired above the Porquerolles Island (France). The retrieval performance of all in-water and seabed parameters derived from the inversion of BIODIVERSITY-like data is compared with the performance obtained using ENMAP and HICO spatial and radiometric specifications. It is shown that a BIODIVERSITY-like sensor significantly improves the estimation performance of the water column parameters. Furthermore, BIODIVERSITY-like sensor is highly appropriate for seabed mapping when bottom pixels are composed of pure material (e.g., Sand or *Posidonia*) in shallow waters when seabed depth is less than 10 m. Conversely, the performance of the inversion deteriorates when seabed pixels are composed of mixed materials (e.g., Sand mixed with *Posidonia*). It is also shown that the concentration of chlorophyll, SPM and CDOM absorption are less sensitive to noise level than depth and seabed abundance.**

***Index Terms*—Bathymetry, hyperspectral, ocean color, radiative transfer, seabed mapping.**

Manuscript received July 20, 2020; revised September 23, 2020; accepted October 13, 2020. Date of publication October 21, 2020; date of current version January 6, 2021. The TOSCA/HYPCOLAC project was supported by French Spatial National Agency (CNES). The data campaign was also supported by the ANR/DGA (French Research Agency/French Defense Agency), on the behalf of the HypFoM under Project ANR-15-ASTR-0019. *(Corresponding author: Audrey Minghelli.)*

Audrey Minghelli and Sayoob Vadakke-Chanat are with CNRS, SeaTech, LIS laboratory, Université de Toulon, 83041 Toulon, France (e-mail: minghelli@univ-tln.fr; sayoob.vadakke-chanat@univ-tln.fr).

Malik Chami is with INSU-CNRS, LATMOS, Sorbonne Université, 06300 Nice, France (e-mail: malik.chami@upmc.fr).

Mireille Guillaume is with CNRS, Centrale Marseille, Institut Fresnel, Aix Marseille Univ., 13013 Marseille, France (e-mail: mireille.guillaume@fresnel.fr).

Marion Peirache is with Parc National de Port-Cros, 83406 Hyères Cedex, France (e-mail: marion.peirache@portcros-parcnational.fr).

Digital Object Identifier 10.1109/JSTARS.2020.3031729

I. Introduction

THERE is a growing interest in the use of hyperspectral imagery, in the field of ocean optics along with the deployment of new hyperspectral satellites [1]. Hyperspectral imagery offers numerous advantages including the spectroscopic techniques for analyzing the remote signal which allows a better understanding of water optical properties even in turbid waters [2]. A hyperspectral resolution allows more accurate determinations of water bio-optical properties because it enables the individual spectral signatures of the hydrosols and seabed features to be detected through the measurements at narrow bands [1], [3], [4]. Furthermore, the recent interest in hyperspectral imagery is amplified by the fact that it allows estimations of geophysical products over different geographic sites, in open as in coastal waters, without needing to have previously chosen the location of bands [5]. This is in conjugation with the growing scientific interest in differentiating certain phytoplankton species/groups and characterizing seabed composition. Consequently, further studies in the field of hyperspectral imagery are necessary [6].

For research on coastal waters and inland freshwater benthic habitats, this technique has been extensively exploited. For shallow waters, the determination of bathymetry as well as the composition of the benthic vegetation can be carried out based on ocean color technology. A water body is called optically shallow when the above water reflectance can be determined by the optical properties of the water column, seafloor, and the depth [7]. Knowledge of the benthic vegetation is important for the characterization of marine habitats [8]. Habitats are distinct bio-physio-geo-chemical environment regions in contrast to neighboring areas [9]. Studies using remote sensing performed to date in the optically shallow waters have generally attempted to map the spatial distribution of single benthic habitats or habitats with a single dominant species or multiple heterogeneous habitats (seagrasses, macroalgae, or coral reefs). Studies have also been conducted on the temporal dynamics of the benthic habitats which aid in the understanding of variations in environmental conditions [10]. Bathymetry estimation is one of the research topics where remote sensing applications have been most frequently used. Thus, the remote sensing technique plays an important and expanding role in ocean applications [10].

The vast majority of the signal received at the satellite level is caused by the atmospheric scattering [11], that contributes to about 80%–90% [12] of the total signal in oceanic waters. Furthermore, part of the radiation reaching the sensor comes from the skylight and sunlight reflections onto the sea surface, which is often called the glint signal. Both the atmospheric and glint radiances need to be removed from the satellite data, which is the so-called atmospheric correction procedure. The part of incident light entering into the water column that is absorbed and scattered away does not reach the remote sensing detector. The radiation that interacts with water and constituents and scatters back to the atmosphere contains useful information about the water column but not from the seabed. Only the part of the radiation that reaches the seabed and reflects up to the sensor contains information about the bottom.

For nearly two decades, there has been an increase in the use of hyperspectral airborne images combined with the use of exact radiative transfer models, such as Hydrolight, [13] or semi-analytical models such as Lee's [14] to determine the water bio-optical properties, namely the Chlorophyll-a concentration (*Chl*), the suspended particulate matter (SPM) concentration and the absorption coefficient of the colored dissolved organic matter (*CDOM*), and the seabed features, such as bathymetry and composition. The analysis of the propagation of light through the water column is carried out using radiative transfer models that link the remote sensing reflectance to the properties of the optically active water constituents. Different methods have been developed for the seabed characterization. Some methods use the correction of the water column attenuation [15] or look-up table of seabed reflectance [16]. The inversion of a semi-analytical model can also be used to estimate the water column parameters, the abundance of bottom classes, and the seabed depth [17].

The abundance within each pixel using remote sensing in the optically shallow waters was rarely estimated for practical considerations due to the extensive field calibrations that are required by the estimation models [18]–[22]. More recently, the significance of benthic vegetation in the global carbon budget of the oceans has been getting wider recognition while it has been largely ignored in the past [23]. Therefore, more studies were undertaken with the goal of quantifying the productivity of benthic habitats using remote sensing technology as well as the mapping and abundance estimation [24], [25].

The potential of remote sensing techniques in obtaining information from the seabed for shallow waters is promising though it is more difficult as compared with terrestrial targets. The exploitation of the seabed spectral information is made more challenging because of the influence of the water column on the light propagation from the sea surface to the bottom. As a consequence, the radiation that reaches the remote sensor is attenuated by both the water column and the atmospheric layers.

Various hyperspectral sensors are available but most of them are mounted on an airborne platform, such as CASI, AVIRIS, HYSPEX, which are characterized by a good spatial resolution and a good signal to noise ratio (SNR). Only a very small number of sensors are mounted on a satellite platform. As examples, hyperspectral imager for the coastal ocean (HICO) (90 m, 87 bands) was onboard the International Space Station, operated by NASA, between 2009 and 2014, PRISMA (30 m, 250 bands) [26] was launched in March 2019 by ASI, environmental mapping and analysis program (ENMAP) (30 m, 88 bands) is planned to be launched in 2020 by DLR, and a BIODIVERSITY-like sensor (8 m, 53 bands) is planned to be launched in the future by CNES (French space agency) [27]. PACE-OCI (1 km, 118 bands) is a moderate spatial resolution hyperspectral sensor that is planned to be launched in 2022. Three parameters are decisive for the analysis of these data: the spatial and spectral resolutions, and the SNR. Note that a BIODIVERSITY-like sensor is more sophisticated in terms of spatial resolutions (8 m) and SNR than the existing hyperspectral sensors. The objective of this article is to evaluate the benefit of a BIODIVERSITY-like sensor for determining the water column parameters and for characterizing the seabed depth and composition in coastal zones. The results obtained are compared with ENMAP and HICO sensor performances. The rest of the article is organized as follows: the study area in Porquerolles Island, the *in situ* and hyperspectral data and the methodology of simulation are described in Section II. The results of inversion of BIODIVERSITY simulation are presented in Section III and discussed in Section IV in comparison with other hyperspectral satellite sensors performances.

Fig. 1. Study area of Porquerolles Island (France) and *in situ* sampling stations measurements (red square).

II. Data and Method

A. Study Area

The study area is the coastal water of Porquerolles Island, south-eastern France (see Fig. 1). The island is a sanctuary and a part of the National Park of Port-Cros. The seafloor is characterized by seagrass, sand, and algae covers. The seagrass in the region belongs to the endemic species *Posidonia oceania*, while the algal species is *Caulerpa taxifolia*, a tropical invasive algae carried to the Mediterranean Sea by the Atlantic Ocean currents. Note that the first appearance of *Caulerpa taxifolia* occurred 3 decades ago [28], [29]. The photophilic algae of the species *Cystoseira Amentacea* are also observed in the seafloor rocks [30].

B. Data

The airborne data acquisition campaign was conducted on September 13, 2017. The date was selected taking into account that summer is the best season to observe *Caulerpa taxifolia* due

Fig. 2. Hyperspectral image acquired by the HYSPEX sensor above the study area on September 13, 2017.

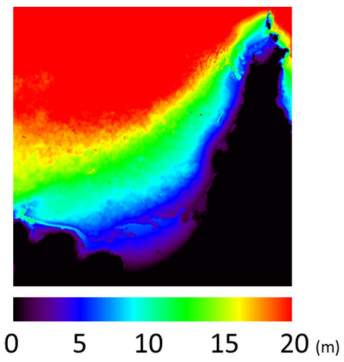

Fig. 3. Litto3D modeled bathymetry for the study area.

to its seasonal cycle. The airborne HYSPEX sensor, operated by Hytech Imaging, was used to obtain hyperspectral images (see Fig. 2). At an altitude of 2666 m, the spatial resolution of the sensor is 1 m [31]. It provides 160 spectral bands between 400 and 1000 nm at 3.6 nm intervals. The atmospheric correction procedure was performed using the ATCOR algorithm [32]. Targets were fixed on the ground in the field of view of the sensor to adjust the atmospheric correction process. Ground targets consisted of black, grey, and cream fabric, each covering an area of 5 m^2. The cream color was chosen to avoid saturation of the radiance in the image. Their hyperspectral reflectance was measured in the laboratory prior to their deployment in the field. The weather conditions during the field experiment were windy with wind speed values between 10 and 15 m s^{-1}. The resulting sea surface roughness caused the sunlight reflection on the sea surface (i.e., so-called sun glint) to affect the airborne data. A correction procedure for the sunglint radiance was thus performed using the signal measured in the near-infrared bands (one band between 800 and 900 nm) where the water reflectance is considered to be null [33]. The Litto3D data [34], which were obtained from a LIDAR (light detection and ranging) campaign carried by the SHOM (hydrographic and oceanographic department of the marine office) and the IGN (national geographic institute) French institutes in 2015, provide a bathymetric model with a 1 m resolution and a precision of 95% (see Fig. 3). These data were used for bathymetry validation in this study.

A portable ASD Handheld2 sensor was used to collect the reflectance spectra for observing the abundance of the bottom

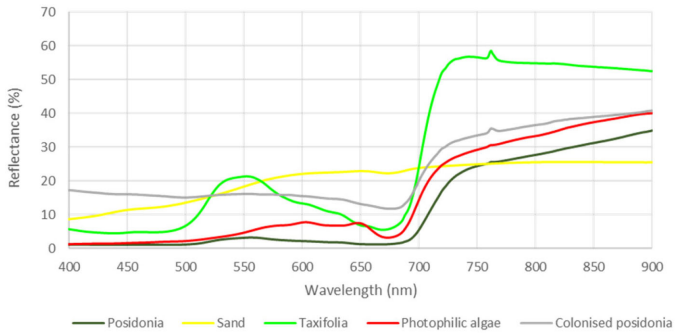

Fig. 4. *In situ* measurements of the hyperspectral reflectance of the various components of the seabed, namely the seagrass, sand, and algae.

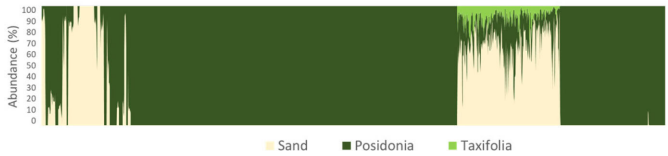

Fig. 5. Proportion of each class composing the seabed, namely Sand, *Posidonia*, and *Caulerpa taxifolia* within a 1 m square resolution on the transect between the sampling stations 1 and 4.

classes. The spectral resolution of the sensor is 1 nm and the spectral range of measurements is from 350 to 1000 nm. The individual reflectance spectra of the seabed composition classes, namely Algae, Seagrass, and Sand, were measured on the boat using samples taken from the seabed by a diver. The resulting reflectance spectra showed that algae and seagrass spectra exhibit a reflectance increase around 700 nm, which is typical of vegetation targets (see Fig. 4). The sand reflectance gradually increases with wavelength. *Caulerpa taxifolia* shows a pronounced peak at 550 nm because of its light green color. *Posidonia* has a seasonal cycle. On spring, new dark green leaves grow. During the summer, some leaves are colonized by epiphytes algae and the color can become lighter.

Underwater Red-Green-Blue images were obtained by the Vortex Remotely Operated Vehicle (ROV) of IFREMER (French research institute for the exploitation of the sea) for a given transect between stations 1 and 4 over a distance of 1500 m. The resolution of the Nikon D5200 camera is 6000 × 4000 pixels, the spatial resolution of each pixel is 2.3 cm. All the images making up the mosaic were classified into 3 classes (Sand, *Posidonia*, and *Caulerpa taxifolia*). The photophilic algae, located on the rocks are absent on this transect. The proportion of each class within 1 m square along the transect was calculated. A profile can then be obtained with the proportion of each class on the transect from station 1 to 4 (see Fig. 5) and can be used to validate the seabed mapping obtained with the simulated images.

The water column inherent optical properties and the concentration of water constituents were also measured for 6 selected stations (see Fig. 1). The backscattering coefficients at 3 wavelengths (440, 532, 650 nm) were measured using the ECO-BB3 instrument from WETLabs/SeaBird (USA). The absorption and attenuation coefficients were measured using the *ac-s* meter from WETLabs/SeaBird (USA), which measures the spectra at

TABLE I
IN SITU MEASUREMENTS OF WATER COLUMN PARAMETERS

Station	Chl (mg/m^3)	SPM (g/m^3)	CDOM (m^{-1})	Depth (m)
1	0.265	0.46	0.01	2.73
2	0.481	0.44	0.01	10.15
3	0.485	0.21	0.01	11.83
4	0.433	0.65	0.06	9.74
5	0.447	0.69	0.01	24.04
6	0.413	0.47	0.01	15.33

4 nm intervals. The *chl* concentration was measured along the water column using the multiparameter data probe HYDROLAB DS5 equipped with a fluorometric probe. The values were averaged over the water column for each station. *SPM* and *CDOM* were also measured by collecting field samples 1 m beneath the sea surface. For SPM measurements, water samples (2l) were filtered and weighed. For *CDOM* measurements, 60 ml water samples were collected and the absorbance was measured in the laboratory using a spectrometer equipped with a double beam monochromator; the excitation wavelengths are between 220 and 600 nm with 0.2 nm resolution (UV 1800 Shimadzu).Depth was measured with the sounder of the boat (CLIPPER NASA Marine) and corrected for the sea level [35]. Chlorophyll concentration, SPM, CDOM and depth for each station are given in Table I. The *in situ* measurements are only used for validation purpose.

C. Methodology

The first part of the study is dedicated to the analysis of radiative transfer synthetic data to investigate the sensitivity of the various tested hyperspectral satellite sensors on the estimation of the water and seabed optical properties. The second part of study is dedicated to the simulation of a satellite image from aerial hyperspectral images.

1) Simulations Using Synthetic Data: Lee's model [14] is used to simulate remote sensing reflectance for three water types (clear, moderately turbid, and turbid), with a depth (Z) varying between 1 and 20 m, and for 45 configurations of the seabed composition that consist of various combinations of 1, 2, or 3 materials taken from among five classes, namely sand, fresh *Posidonia*, colonized *Posidonia*, *Taxifolia*, and photophilic algae. a_i corresponds to the abundance of the bottom i. Clear waters correspond to $Chl = 0.3$ mg.m^{-3}, $SPM = 1$ g.m^{-3}, $CDOM = 0.01$ m^{-1}, moderately turbid waters to $Chl = 1$ mg.m^{-3}, $SPM = 10$ g.m^{-3}, $CDOM = 0.07$ m^{-1}, and turbid waters to $Chl = 5$ mg.m^{-3}, $SPM = 30$ g.m^{-3}, $CDOM = 0.2$ m^{-1}. The satellite sensor data are also simulated (spatial resolution, bands and noise) and an error due to the atmospheric correction is taken into account. Then, the inversion of the simulated satellite radiances is performed to determine the error of estimation of both water column parameters the seabed abundance (a_i') and the seabed abundance (*Chl'*, *SPM'*, *CDOM'*, *and Z'*). The flowchart showing the method used for performing the simulations is presented in Fig. 6.

2) Simulation With Airborne Hyperspectral Imagery: The second part of the study consists of simulating a BIODIVERSITY-like image to compare the retrieved estimations of the bio-optical parameters (e.g., SPM and *Chl*, depth) and of the seabed abundance with various types of data such as the *in situ* measurements, the airborne HYSPEX data and the data that will be retrieved from satellite hyperspectral sensors such as ENMAP and HICO (see Fig. 7).

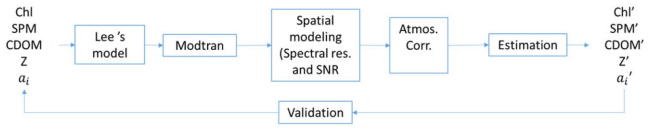

Fig. 6. Flowchart of the method used for performing the theoretical simulations.

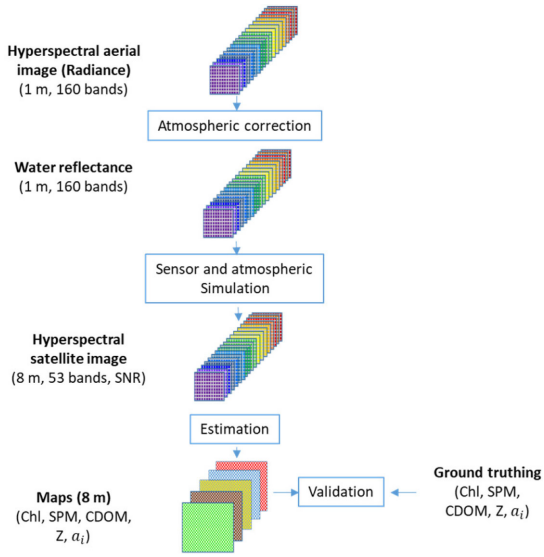

Fig. 7. Flowchart scheme of the method used for determining the water and seabed properties from airborne data.

The input dataset is the hyperspectral aerial image with 1 m and 160 spectral bands between 400 and 1000 nm acquired with the HYSPEX sensor. This image was corrected for the atmospheric effect to obtain water reflectance. The atmospheric contribution was added to simulate the atmospheric effect from the surface level to the satellite level to obtain a top of atmosphere radiance. The spatial resolution and the spectral configuration of the airborne hyperspectral image are degraded to match with the satellite sensors specifications (BIODIVERSITY, ENMAP, and HICO); the sensor noise is also added. The simulated satellite image is then corrected for the atmospheric effects to derive the water reflectance, taking into account uncertainties due to the atmospheric corrections. The result of the inversion of the satellite radiance can then be compared to *in situ* measurements at the sea surface level as shown in Fig. 7. The details of the different steps are given in the following paragraphs.

3) Lee's Model: The semi-analytic model used in this study is the model developed by Lee *et al.* [14]. This model provides the remote sensing reflectance (denoted *Rrs*) as a function of the water composition (chlorophyll concentration, *SPM* concentration, *CDOM* absorption coefficient at 440 nm, the depth and the abundance of the material composing the seabed). Inherent

optical properties are calculated as the nonwater absorption coefficient $[a_{\mathrm{nw}},\ (1)]$ and the backscattering coefficient $b_b(2)$. $a^*_{\Phi},\ a^*_{NAP},\ b^*_{b\Phi},\ b^*_{bNAP}$, are the constituent specific absorption or backscattering coefficients, and $s_{\mathrm{CDOM}},\ s_{\mathrm{NAP}}, y_{\Phi}$, and y_{NAP} are the spectral slopes of the optical properties of these constituents, respectively. Φ stands for phytoplankton pigments and NAP stands for nonalgal particle. The standard values of specific inherent optical properties given in [36] were used in this study because this study site consists of clear water type. The measurement of backscattering coefficients, absorption and attenuation coefficients were used to check that the backscattering and absorption coefficients calculated by the model were consistent with the standard constant values used. The reflectance of the water column and seabed are $r_{rs}C$ and $r_{rs}B$, respectively (4). The seabed reflectance (ρ_b), as given in (3), is a linear relationship between abundance and reflectance of each seabed class within the pixel. a_s, a_p, a_{cp}, a_t, a_a are respectively the abundance of sand, *Posidonia*, colonized *Posidonia*, *Caulerpa taxifolia*, photophilic algae and ρ_s, ρ_p, ρ_t, and ρ_a are respectively the reflectance of each class which are considered known. The sum of abundance is considered to be 1

$$a_{\mathrm{nw}}\ (\lambda) = \mathrm{Chl} * a^*_{\Phi}\ (\lambda) + \mathrm{CDOM} * e^{-S_{\mathrm{CDOM}}(\lambda - 440)}\ (\lambda) + \mathrm{SPM} * a^*_{\mathrm{NAP}}\ (440)\, e^{-S_{\mathrm{NAP}}(\lambda - 440)} \quad (1)$$

$$b_b\ (\lambda) = b_{\mathrm{bw}}\ (\lambda) + \mathrm{Chl} * b^*_{b\Phi}\ (542) \left(\frac{542}{\lambda}\right)^{Y_{\Phi}} + \mathrm{SPM} * b^*_{b\mathrm{NAP}}\ (542) \left(\frac{542}{\lambda}\right)^{Y_{\mathrm{NAP}}} \quad (2)$$

$$\rho_b\ (\lambda) = a_s\ \rho_s\ (\lambda) + a_p \rho_p\ (\lambda) + a_{cp} \rho c_p\ (\lambda) + a_t \rho_t\ (\lambda) + a_a \rho_a\ (\lambda) \quad (3)$$

$$r_{rs}\ (\lambda) = r_{rs}C + r_{rs}B \quad (4)$$

$$R_{rs}\ (\lambda) = \frac{0.52\ r_{rs}\ (\lambda)}{1 - 1.56\ r_{rs}\ (\lambda)}. \quad (5)$$

The $r_{rs}C$ and $r_{rs}B$ depends on the depth parameter (Z). The higher the depth, the greater $r_{rs}C$, and the lower $r_{rs}B$ and *vice-versa*. The reader is referred to [14] for more details about the model and the equations.

4) Simulation of the Atmosphere: The atmospheric radiative transfer model MODTRAN is used to simulate the radiance at the top of the atmosphere. The Mid-latitude (45°N) summer model is selected as the atmospheric model and the marine aerosol is selected as the aerosol model with a visibility of 40 km. For the geometric configuration, the solar zenithal angle (θ_s) was set to 40°, the viewing zenithal angle (θ_v) at 0°, and the difference of azimuthal angles $\Delta\phi$ at 167°, which is the relative azimuth value of the airborne measurements acquired in this study. The outputs of the MODTRAN simulation are the atmospheric reflectance, the spherical reflectance, and the direct and diffuse transmittance. The TOA reflectance (ρ_{TOA}) and the TOA radiance (L_{TOA}) can then be calculated using (5) and (6)

$$\rho_{\mathrm{TOA}} = \rho_{\mathrm{atm}} + \frac{t^{\downarrow}}{1 - \rho_{\mathrm{sph}} \cdot \rho_e} \left(t^{\uparrow}_{\mathrm{dir}} \cdot \rho_w + t^{\uparrow}_{\mathrm{dif}} \cdot \rho_e\right) \quad (6)$$

TABLE II
SPECTRAL AND SPATIAL RESOLUTIONS OF THE HYPERSPECTRAL SENSORS EXAMINED IN THIS STUDY

Sensor	Total number of bands/number of bands in the range [400-700 nm]	FWHM (nm)	Domain (nm)	Spatial resolution (m)
HYSPEX	160/79	4,5	404-990	1 m
Biodiversity	53/26	10	413-990	8 m
ENMAP	88/43	8.2	415-1000	30 m
HICO	87/50	10	410-1000	90 m

Note: FWHM is the full width half maximum.

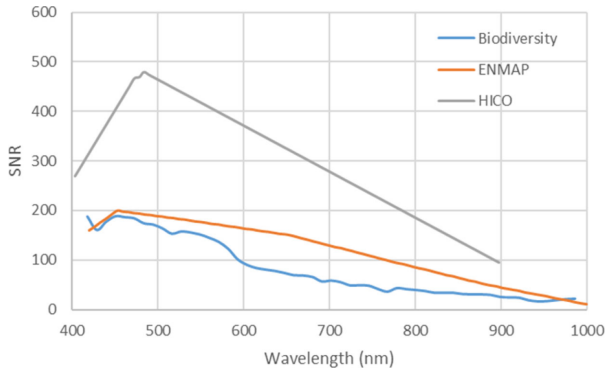

Fig. 8. Signal-to-noise ratio (SNR) values used for the three sensors.

where ρ_{atm} is the atmospherical reflectance, ρ_{sph} is the spherical atmospheric reflectance, $t^{\downarrow}$ is the downwelling transmittance, $t^{\uparrow}_{\mathrm{dir}},\ t^{\uparrow}_{\mathrm{dif}}$ are the upwelling direct and diffuse transmittance, and ρ_e is the environmental reflectance

$$L_{\mathrm{TOA}} = \frac{1}{\pi}\ \cdot \cos\theta_s \cdot F_0 \cdot \rho_{\mathrm{TOA}} \quad (7)$$

where θ_s is the solar zenithal angle (40°), and F_0 the is the solar irradiance given by MODTRAN [38].

5) Consideration of the Sensor Radiometric and Spectral Specifications: The monochromatic simulated reflectances are averaged over the spectral bands of the satellite sensor (see Table II). The SNR simulation is operated by adding to the top of atmosphere radiance a Gaussian noise with a null mean value and a standard deviation provided for the sensor at the given band (7).

The BIODIVERSITY-like noise was calculated based on (8). The values of $\alpha(\lambda)$ and $\beta(\lambda)$ were provided by the CNES for all the 88 spectral bands [39]

$$\sigma_{\mathrm{sensor}}\ (\lambda)\ = \sqrt{\alpha(\lambda)^2 + \beta\ (\lambda) \cdot L_{\mathrm{TOA}}}\ . \quad (8)$$

The SNR of the BIODIVERSITY-like sensor, ENMAP, and HICO are shown in Fig. 8. The SNR of ENMAP and HICO sensors were obtained from the literature [40], [41] for a given spatial resolution of the sensor. Note that the BIODIVERSITY

SNR values are consistent with the recent recommendation of the scientific community requirement for future hyperspectral sensors through the CEOS report [42]. They cannot be compared to each other without taking into account the resolution information. The standard deviation of the noise is obtained by dividing the radiance L_{TOA} by the SNR. For the simulation with airborne hyperspectral imagery, the spatial resolution is obtained by spatially averaging and down sampling the image to obtain the required spatial resolution.

6) Atmospheric Correction Simulation: To take into account an error due to the atmospheric correction, two other noises are added to the simulated reflectance. One is due to the error made on the surface reflectance retrieval and one is due to the error made on the aerosol model. The details of simulation are given in [43].

7) Estimation of Seabed and Water Optical Properties: The inversion of the water reflectance is achieved by minimizing the Euclidian distance between the model and the measured reflectance of each pixel of the image through optimization. The minimization is operated by a nonlinear curve-fitting in least-squares sense using the "lsqcurvefit" MATLAB function with bounds for each parameter. The outputs of the inversion are the optimized values of *Chl*, *SPM*, CDOM, depth, and the seabed abundances of sand, *Posidonia*, colonized *Posidonia*, *Caulerpa taxifolia*, and photophilic algae for each pixel. At the end of the inversion process, the spatial distribution of *Chl*, SPM, CDOM, depth, and seabed abundances of sand, *Posidonia*, *Taxifolia*, and photophilic algae are then obtained.

D. Validation

All the estimated seabed and water parameters are compared with validation data. The metrics of the root mean square error (RMSE) and the relative error (*RE)* (9) are used to quantify the performance of the retrieval

$$RE\ (\%) = \frac{abs\left(\hat{P} - P_{ref}\right)}{P_{ref)}} * 100 \qquad (9)$$

where $\hat{P}$ *is* the estimated parameters and P_{ref} the desired values.

III. Results

A. Theoretical Simulations

First, the influence of the seabed depth on the retrieval performance of each parameter is analyzed. About 100 simulation runs were carried out for each case to provide relevant statistics. Fig. 9 shows the relative error on the retrieval of SPM concentration when using a BIODIVERSITY-like sensor configuration for three water turbidities, namely clear, moderately turbid, and turbid waters. The relative error decreases with the seabed depth because of the stronger influence of the water column relative to the influence of the seabed, which leads to an improvement in the performance of the SPM retrieval. The relative error also decreases with turbidity. This is because the influence of the SPM on the sub-surface reflectance is greater. The relative error on SPM could reach 100% in very shallow waters. It is lower than 40% for moderately turbid waters and lower than 20% for turbid waters.

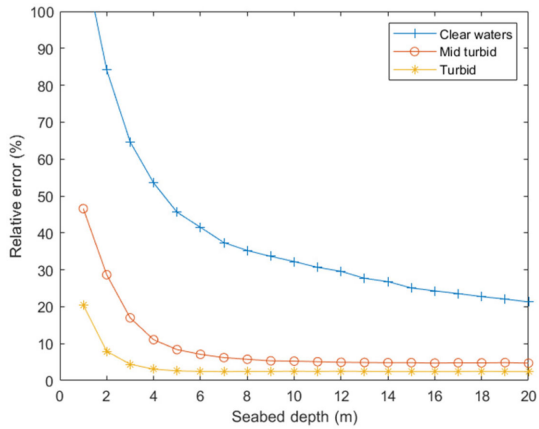

Fig. 9. Variation of the relative errors of the estimated SPM concentration with the seabed depth and water turbidity when a BIODIVERSITY-like sensor configuration is used.

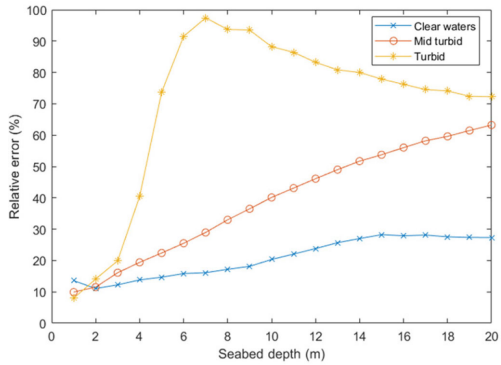

Fig. 10. Variation of the relative errors of the estimated seabed depth with bathymetry and water turbidity when a BIODIVERSITY-like sensor configuration.

The variations of the relative error on the chlorophyll and CDOM retrieval performances with bathymetry and water turbidity (not shown here) are similar to those observed for SPM. Typically, the relative error on the chlorophyll estimation is greater than 70% in clear waters, around 30% in moderately turbid waters, and less than 10% in turbid waters. The relative error on CDOM absorption coefficient at 443 nm is higher than 50% in clear waters, lower than 30% for moderately turbid water and around 10% in turbid waters.

The relative error that is obtained for the retrieval of the seabed depth regularly increases with bathymetry from 10% to 30% and from 10% to 60% for clear and moderately turbid waters, respectively, for depths ranging between 1 and 20 m (see Fig. 10). Interestingly, the relative error remains lower than 30% for clear waters including for a seabed depth of 20 m for which the retrieval is often considered as challenging. For moderately turbid waters, higher values of the relative error than the clear water case are expected because the hydrosols mostly contribute to the sea surface reflectance for deeper waters. The relative errors found for the turbid water case sharply increase from 10% to 80% up to 6 m depth as a result of the increase of the influence of the hydrosols on the light scattering reaching the sea surface. Beyond 6 m depth, the seabed reflectance no longer influences the surface reflectance and the absolute error reaches

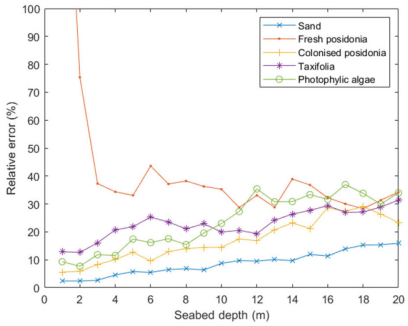

Fig. 11. Variation of the relative errors of the estimated seabed depth with bathymetry for various seabed compositions and for clear water, when a BIODIVERSITY-like sensor configuration is used.

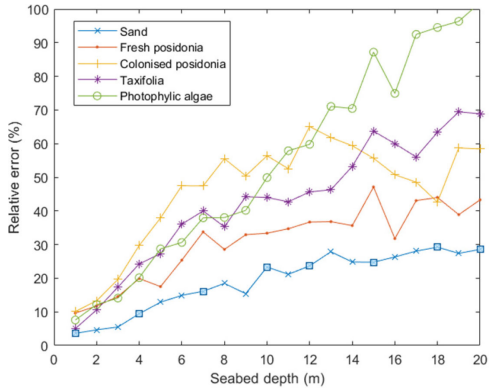

Fig. 12. Variation of the relative errors of the estimated seabed material abundance (in %) with bathymetry for seabed composed of pure materials in clear water, when a BIODIVERSITY-like sensor configuration is used.

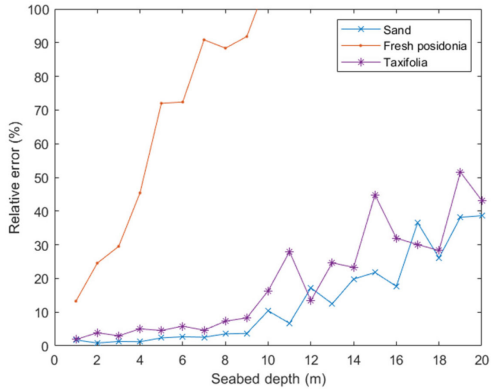

Fig. 13. Variation of the relative errors of the estimated seabed material abundance (in %) with bathymetry for seabed composed of mixed materials, namely 1/3 of Sand, 1/3 of fresh Posidonia, 1/3 of Caulerpa taxifolia species for BIODIVERSITY-like sensor configuration.

TABLE III
COMPARISON OF RMSE CALCULATED FOR THE ESTIMATED WATER COLUMN PARAMETERS AND SEABED MATERIAL ABUNDANCES IN CLEAR WATERS USING VARIOUS HYPERSPECTRAL SATELLITE SENSORS

Sensor	Biodiversity	Biodiversity	ENMAP	Biodiveristy	ENMAP	HICO
Spat. Res.	8m	30m	30m	90m	90m	90m
Spect. Res.	26 bands	26 bands	43 bands	26 bands	43 bands	50 bands
Chl ($mg.m^{-3}$)	0.5687	0.2782	0.4361	0.1018	0.2159	0.4584
SPM($g.m^{-3}$)	0.5863	0.2796	0.3525	0.1477	0.1920	0.5925
CDOM (m^{-1})	0.0223	0.0056	0.0124	0.0023	0.0048	0.0106
Z (m)	4.1775	1.7717	2.6241	0.9158	1.3277	2.9958
Sand	0.2278	0.1269	0.1626	0.0913	0.1125	0.1536
Fr. *Posidonia*	0.5037	0.4132	0.4537	0.3248	0.3699	0.4799
Col. *Posidonia*	0.3812	0.2815	0.3374	0.2043	0.2525	0.3322
Caulerpa taxifolia	0.3194	0.1970	0.2314	0.1251	0.1415	0.2427
Phot. Algae	0.7732	0.4453	0.5505	0.2744	0.3386	0.5145

an asymptotic value. Note that since the relative error is obtained by dividing the absolute error by the actual depth, the relative error shows a decrease beyond 6 m depth.

The relative error is also analyzed with respect to the seabed composition (see Fig. 11) in the clear water case. The seabed depth is much better retrieved for bright targets such as sand and colonized *Posidonia* than for dark targets such as the fresh *Posidonia*.

The relative errors obtained for the retrieval of the seabed material abundance are shown in Fig. 12 for the case of a seabed composed of a pure material and Fig. 13 for the case of a seabed composed of mixed materials. The error increases with depth as a result of the increasing influence of light scattering by hydrosols of the water column (see Fig. 12). The material abundance is also better estimated on bright targets (Sand) than on dark target (*Posidonia*).

A pixel composed of mixed material (e.g., 1/3 Sand, 1/3 fresh *Posidonia* and 1/3) also demonstrates that the seabed material abundance is better estimated on bright target (sand and *Caulerpa taxifolia*) than on dark target (fresh *Posidonia*) (see Fig. 13). In particular, in clear water, the errors are lower than 5% when the bathymetry is lower than 10 m. Note that the performance of the retrieval significantly deteriorates for Fresh *Posidonia* where the error rapidly increases up to 100% when the bathymetry is higher than 6 m. Thus, a dark target is not well determined for deep waters.

Table III presents the RMSE on the estimation of water column parameters and seabed material abundances in clear waters for a BIODIVERSITY-like sensor and other sensors including ENMAP, and HICO. If the noise level (SNR) is given for a resolution noted R, the noise level at a coarser resolution (noted R') is given by $SNR' = SNR/(R'/R)$. Then $R' > R$ and $SNR' > SNR$. The band features of the sensors are simulated by integration between 400 and 700 nm.

It is observed that the RMSE decreases with the spatial resolution of the sensor (see first 2 columns of Table III, which is likely to be due to the averaging effect on the noise. For the given spatial resolution of 30 m, lower values of RMSE are obtained for the BIODIVERSITY-like sensor relative to the ENMAP sensor because of its SNR. The RMSE obtained for ENMAP is lower than HICO for a spatial resolution of 90 m while the BIODIVERSITY like sensor performs better than both ENMAP and HICO for all the parameters for the same spatial resolution. Finally, when the resolution and the SNR are fixed, the RMSE increases when the number of bands decreases. When the number of bands and the SNR are fixed, the RMSE decreases when the spatial resolution decreases. When the spatial and the spectral resolution are fixed, the RMSE increases when the SNR decreases. But as the SNR of the BIODIVERSITY-like sensor is better than ENMAP's and HICO's at the same spatial resolution, the RMSE is lower with BIODIVERSITY's 26 bands than with ENMAP'43 bands or HICO's 50 bands. This means that a high SNR can balance with a low number of bands and inversely.

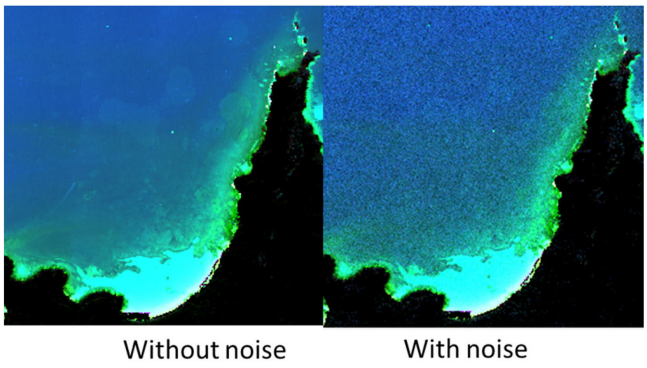

Fig. 14. Color composite of the simulated BIODIVERSITY-like image without and with noise (bands 440, 552, 680 nm).

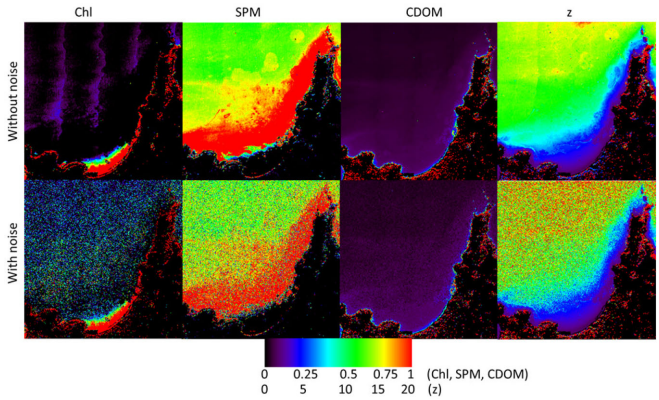

Fig. 15. Retrieved maps of water column parameters and bathymetry derived from the inversion of the airborne data once they have been propagated to the satellite level: (top) for noise-free data, (bottom) for noisy data.

TABLE IV
ABSOLUTE ERROR (AE) AND RELATIVE ERROR (RE) OF THE RETRIEVED WATER COLUMN AND BATHYMETRY PARAMETERS CALCULATED USING THE *IN SITU* MEASUREMENTS COLLECTED OVER THE SIX SAMPLING STATIONS FOR THE CASES WHERE THE NOISE IS ACCOUNTED FOR IN THE DATA

Station	Chl ($mg.m^{-3}$)		SPM ($g.m^{-3}$)		CDOM (m-1)		Depth (m)	
	AE	RE (%)	AE	RE (%)	AE	RE (%)	AE	RE
1	0.392	148%	-0.310	-67%	0.077	771%	-0.790	-29%
2	0.389	81%	-0.333	-76%	0.088	879%	2.899	29%
3	0.417	86%	-0.108	-52%	0.075	745%	3.808	32%
4	-0.413	-95%	0.451	69%	0.034	56%	3.015	31%
5	-0.427	-96%	0.412	60%	0.075	752%	-5.490	-23%
6	-0.403	-98%	0.777	165%	0.064	636%	-3.554	-23%
Total	**0.407**	**101%**	**0.446**	**81%**	**0.071**	**640%**	**3.545**	**28%**

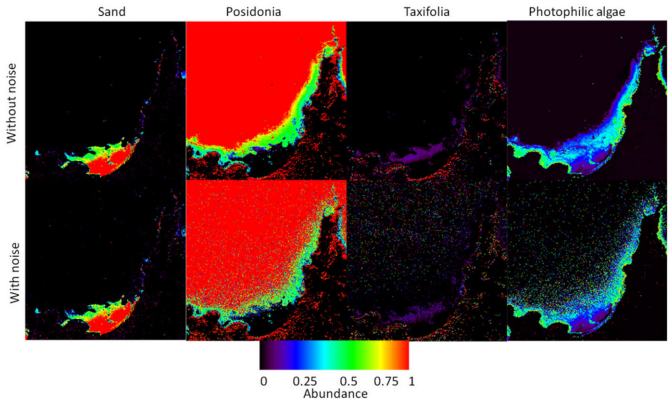

Fig. 16. Retrieved abundance of seabed materials, namely Sand, *Posidonia*, *Caulerpa taxifolia*, and photophilic algae, from the inversion of satellite data simulated for the BIODIVERSITY-like sensor configuration.

B. Satellite Simulation With Airborne Data

The BIODIVERSITY-like simulated image is shown in Fig. 14 without and with noise. Even low, noise is visible because the land has been removed from the images and a linear histogram stretch has been applied on the water area.

The retrieved maps of water quality parameters derived from the airborne data acquired using the HYSPEX sensor for which the radiance has been propagated to the satellite level by considering both the atmospheric radiance and the BIODIVERSITY-like sensor noise are shown in Fig. 15.

When the noise is ignored in the satellite data, the concentration of *Chl* is low (<0.2 $mg.m^{-3}$) except near the beach (>0.2 $mg.m^{-3}$). The SPM is quite high (>1 $g.m^{-3}$) at intermediate seabed depths, typically between 5 and 10 m. CDOM absorption coefficient is weak (<0.05 m^{-1}) over the whole area. Bathymetry logically increases with the distance from the beach.

The retrieved parameters can be compared with *in situ* measurements. For that purpose, the error and the relative error obtained for each parameter and each station are reported in Table IV.

Note that the absolute error is low for Chl, SPM, and CDOM, while the relative error is high because their concentrations are weak thus not significantly influencing the reflectance; the retrieval performance of these variables with a high degree of accuracy remains challenging using semi-analytical model inversion. Considering the bathymetry, the relative error is lower than the other parameters while the absolute error is high because of the considerable depth of the stations: four of them are depths of over 10 m (see Table I).

Maps of the retrieved seabed material (or classes) are shown in Fig. 16. The materials that are derived from the data are Sand, *Posidonia*, *Taxifolia*, and Photophilic algae. The Sand component is identified close to the beach. *Posidonia* covers the largest area while the occurrence of *Taxifolia* is restricted to a small area. Photophilic algae are located on the rocks which is consistent with in situ observations.

The retrieval of the seabed material abundance using the BIODIVERSITY-like simulated image can be compared with the *in situ* profile (see Fig. 5) acquired using the IFREMER ROV along a transect between the sampling station 1 and 4 (station 1, 2, 3, and 4) in Fig. 1. The four stations (1 to 4) are area of clear water. Fig. 17 shows the measured material abundance (top), the measured bathymetric profile, and the retrieved material abundance from the inversion of the simulated satellite data for the cases where the noise is ignored and taken into account.

The left side of Fig. 17 corresponds to shallow waters (~ 6 m) and the right side corresponds to deep waters (12 m). For the

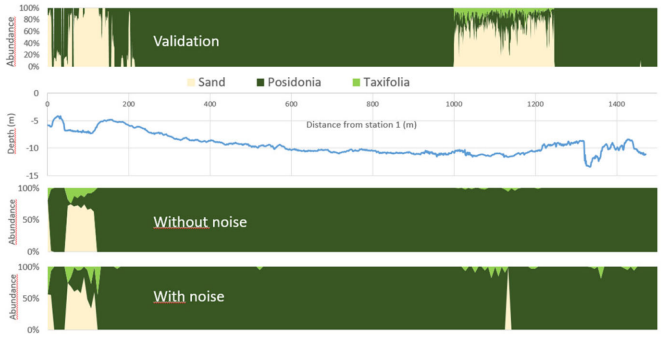

Fig. 17. (top) *In situ* measurements of the seabed material abundances acquired by the ROV (IFREMER) along the transect going from station 1 to station 4, (middle) bathymetry along the transect, (bottom) retrieved seabed composition for the cases where the noise is ignored and taken into account and for satellite data simulated for the BIODIVERSITY-like sensor configuration.

TABLE V
COMPARISON OF THE RMSE FOR THE RETRIEVAL OF WATER COLUMN PARAMETERS (CHL, SPM, CDOM, SEABED DEPTH) BETWEEN THE SIMULATED DATASETS AND THE *IN SITU* MEASUREMENTS COLLECTED IN THE SAMPLING STATIONS

RMSE	Biodiversity degraded to 30m 26 bands	ENMAP 30m 43 bands	Biodiversity degraded to 90m 26 bands	ENMAP degraded to 90m 43 bands	HICO 90m 50 bands
Chl (mg.m^{-3})	0.3900	0.4880	0.4000	0.3200	0.4200
SPM (g.m^{-3})	0.3800	0.4100	0.3600	0.4900	0.5600
CDOM (m^{-1})	0.0700	0.0500	0.0900	0.0800	0.0900
Z (m)	4.1900	6.8100	0.9800	4.5500	5.4300

case where the noise is ignored, the sand component is correctly mapped in shallow waters (<10 m depth), but not in deep waters (>10 m). This is because the sand is mixed with *Posidonia* and *Taxifolia* in deeper waters. *Posidonia* is appropriately classified for all depths because even though *Posidonia* is a dark seabed, pixels are composed of 100% of *Posidonia,* making its detection easier (see Fig. 12). *Taxifolia* is detected even at 10 m depth but its abundance is underestimated. When the noise is taken into account, the seabed components retrieval is not significantly different from the noise-free case.

To compare the BIODIVERSITY-like sensor performances for the estimation of water column parameters with those of other hyperspectral sensors (e.g., ENMAP, HICO), its resolution was downgraded from 8 to 30 m and 90 m. The RMSE values obtained for different spatial and spectral resolutions are calculated (see Table V).

At 30 m resolution, all the parameters are better estimated using the BIODIVERSITY-like sensor configuration than for the ENMAP sensor. Similar conclusions are observed at 90 m resolution when compared with both HICO and ENMAP.

IV. DISCUSSION

Despite multiple limitations, the hyperspectral remote sensing has developed as a potentially promising technology to study marine and freshwater benthic maps as well as bathymetry [10]. The detectable information is restricted within a maximum depth depending on the sensor characteristics and environmental factors.

The results of the synthetic data simulations performed in this study, for which the noise affecting the top of atmosphere data was rigorously taken into account, provide an insight into the maximum possible accuracy and associated errors with the given configuration of the seabed and the sensor characteristics. The simulations with *in situ* data provide a realistic understanding of the accuracy and associated errors for the same configuration of the seabed and the sensor characteristics. An important factor that affects the accuracy of the estimated water column or seabed parameters is the amount of information that the signal contains from the seabed or water column. The stronger the signal from the water column, the more accurate the estimation of the water column parameters; a similar tendency is observed for the seabed abundances. The radiation from the seabed is higher for clearer waters while a higher proportion of the signal from the water column is observed for turbid waters, which explains the RMSE trends in the estimations from the theoretical simulations. Moreover, the amount of individual spectral information contained in the signal also influences the accuracy of estimation. Depth estimation from remote sensing data depends on the physical changes in the spectral radiance that is reflected from the seabed which is correlated with the water depth variation. However, beyond a threshold depth, the increase in depth affecting the benthic reflectance is too small to be resolved by the sensor and inversion models [10], [44].

Nevertheless, the focus of this work was on the simulation of the BIODIVERSITY-like sensor which provided an understanding of its suitability for the estimation of the water column and seabed parameters with the given characteristics such as the position and number of the measurement bands in the spectrum, the spatial resolution and the SNR of the sensor. The goal of this work to evaluate the potential of a BIODIVERSITY-like sensor in comparison with ENMAP and HICO sensors was accomplished as demonstrated in the results. Remarkably, the error in the estimation of the parameters with the BIODIVERSITY-like sensor is generally lower despite having a fewer number of bands as compared to the HICO and ENMAP sensors in the same spectral resolution as can be observed from the results of the theoretical simulations and the satellite simulation using airborne data (see Tables III and V). In this study, the information provided by each sensor (spatial and spectral resolutions and SNR) was analyzed and it has been shown that a high SNR can balance with a low number of bands and *vice-versa*. Note that these results could be degraded if a lower SNR value concerning BIODIVERSITY sensor was used.

The difficulty observed in the estimation of the proportion of bottom classes in seabed mapping when the seabed is composed of multiple classes is associated with the difficulty in separating individual spectral signatures from an already weak signal modulated by the water column attenuation. As the depth increases, the attenuation increases, and the signal is further weakened and thereby larger errors occur in the estimations, which explain the difficulty in estimating the bathymetry for depths higher than 10 m.

The results in this work are remarkable particularly when compared with a recent study that estimated the detectability limits for seabed estimation for the CASI hyperspectral sensor in the complex waters of the Baltic sea [10]. Vahtmäe *et al.* observed that the detectability threshold for the brightest seabed composed of sand was 7.5, 5 m for brighter benthic flora of green macroalgae, and 3 m for darker benthic flora composed of higher plants and brown macroalgae. Moreover, they observed that the bathymetric mapping was possible in the coastal waters of the Baltic Sea up to a maximum of 4 m depth, whereas the BIODIVERSITY sensor can estimate the depth up to10 m with an error lower than 40% even in moderately turbid waters (see Fig. 10). This can be due to the lower sensitivity of CASI to the bottom reflectance. Despite the fact that the BIODIVERSITY-like sensor is a satellite sensor that could observe through a thicker layer of atmosphere and that is designed with more spectral bands than the airborne CASI sensors, the BIODIVERSITY-like configuration is likely to perform better than the CASI sensor in a similar environment." Louchard *et al.* [45] and Mobley *et al.* [16] used spectral classification and a lookup-table based approach to map the benthic habitats and to estimate bathymetry from portable hyperspectral imager (PHILLS) airborne sensors for clear and shallow coastal waters. The current study focused on the viability of a potential satellite attached BIODIVERSITY-like sensor for different water types (by simulation). Louchard *et al.* [45] were able to estimate depth with a mean accuracy of 83% with the airborne sensor, while Mobley *et al.* [16] demonstrated an accuracy of 95.3% on average for constrained inversion and up to 87.4% for unconstrained inversion. Villa *et al.* [46] implemented a rule-based approach for mapping functional types of macrophytes in the seabed and obtained 90.1% accuracy with up to 20% misclassified mixed sands. Kotta *et al.* [47] investigated the measured reflectance spectra of major macrophyte species in the Baltic sea by using hyperspectral datasets and adopted a methodology to allow statistically significant discrimination of spectral signatures of various macrophyte species.

Most studies on seabed mapping to date were performed for shallow waters with a depth of often less than 5 m, while the present study is performed for waters up to 20 m depth. The relatively low errors in depth estimation (<20%, except for *Posidonia* in shallow waters) for depths up to 20 m using the sensor characteristics in this study in conjugation with the inversion model can be a promising approach for bathymetry estimation which is critically important in the fields of navigation safety, planning of marine farming, delimitation of protected areas, engineering of nearshore infrastructures (e.g., Ports and wind energy structures). A synoptic and rapid method such as using hyperspectral remote sensing sensors for the bathymetry chart preparation can aid in situations where the hydrographic survey is difficult. Moreover, it can also help in cost reduction and time efficiency as compared to a shipborne bathymetric survey even when the latter is feasible [48].

Additionally, the ability of the BIODIVERSITY sensor in the benthic habitats mapping as revealed in this study can be expected to have substantial impacts in the ecological studies after a potential setting up of the studied sensor in a satellite platform. The results and the conclusions in this study can be used as advisory with the implications for the new launch of satellite missions taking into consideration the sensor characteristics studied.

V. Conclusion

The present study was conducted using both synthetic data and data from aerial hyperspectral images of the coastal zone of Porquerolles Island (France). The results showed that the BIODIVERSITY-like sensor configuration characterized by 28 spectral bands on the range 400–700 nm (53 bands on the range 400–1000 nm), 8 m resolution, and an SNR of 200 at 400 nm will be able to better estimate the water column parameters including the chlorophyll concentration, the *SPM*, the *CDOM*, and the seabed depth than the retrieval obtained for the ENMAP and HICO spectral and radiometric configurations.

The BIODIVERSITY-like sensor was able to provide estimates of the *Chl, SPM, CDOM*, and depth with low RMSE of 0.41 $mg.m^{-3}$, 0.43 $g.m^{-3}$, 0.06 m^{-1}, and 3.09 m corresponding. respectively to relative errors of 101%, 81%, 640%, and 28%. The absolute error is low for *Chl, SPM,* and *CDOM*, while the relative error is high because their concentrations are weak thus not significantly influencing the reflectance. Considering the bathymetry, the relative error is lower than the other parameters while the absolute error is high because of the considerable depth of the stations: four of them are located at a depth of over 10 m.

The BIODIVERSITY-like sensor will allow the seabed to be mapped for the pixels composed of only one material (e.g., sand or *Posidonia*). The false detections can be reduced, especially for depths of less than 10 m, and remarkably for *Posidonia cover*. Moreover, the abundance estimations are also fairly accurate where less than 25%, 35%, and 45% errors, respectively, for sand, fresh *Posidonia*, and *Caulerpa taxifolia* were observed (see Fig. 12). On the other hand, there were difficulties in retrieving the pixels composed by several materials (e.g., Sand and *Posidonia*). Further work could consist in taking into account the environmental effect of surrounding seabed in the inversion.

Acknowledgment

The authors are grateful to M. Lei (IGN) for the atmospheric simulation, T. Tormos (Onema) and T. Harmel (GET) for their help during the *in situ* campaign and X. Briottet (ONERA) for helpful discussions about the BIODIVERSITY mission.

References

[1] S. Emberton, L. Chittka, A. Cavallaro, and M. Wang, "Sensor capability and atmospheric correction in ocean colour remote sensing," *Remote Sens.*, vol. 8, no. 1, Dec. 2015, Art. no. 1.

[2] E. Louchard *et al.*, "Derivative analysis of absorption features in hyperspectral remote sensing data of carbonate sediments," *Opt. Express*, vol. 10, no. 26, 2002, Art. no. 1573.

[3] D. Odermatt, A. Gitelson, V. E. Brando, and M. Schaepman, "Review of constituent retrieval in optically deep and complex waters from satellite imagery," *Remote Sens. Environ.*, vol. 118, pp. 116–126, 2012.

[4] M. W. Matthews, "A current review of empirical procedures of remote sensing in inland and near-coastal transitional waters," *Int. J. Remote Sens.*, vol. 32, no. 21, pp. 6855–6899, 2011, doi: 10.1080/01431161.2010.512947.

[5] E. L. Hestir *et al.*, "Measuring freshwater aquatic ecosystems: The need for a hyperspectral global mapping satellite mission," *Remote Sens. Environ.*, vol. 167, pp. 181–195, Sep. 2015, doi: 10.1016/j.rse.2015.05.023.

[6] A. Bracher *et al.*, "Obtaining phytoplankton diversity from ocean color: A scientific roadmap for future development," *Front. Marine Sci.*, vol. 4, pp. 1–15, 2017, doi: 10.3389/fmars.2017.00055.

[7] S. Maritorena, A. Morel, and B. Gentili, "Diffuse reflectance of oceanic shallow waters: Influence of water depth and bottom albedo," *Limnol. Oceanography*, vol. 39, no. 7, pp. 1689–1703, 1994, doi: 10.4319/lo.1994.39.7.1689.

[8] P. Nieto, C. A. Mücher, H. W. G. Meesters, J. Clevers, S. T. Glorius, and A. D. Rippen, "Classifying benthic habitats and deriving bathymetry at the Caribbean Netherlands using multispectral imagery," *Wagening. Univ. Res. Cent.*, M.Sc. Thesis, Rep. GIRS-2013-18, pp. 1–98, 2013.

[9] P. C. Valentine, B. J. Todd, and V. E. Kostylev, "Classification of marine sublittoral habitats, with application to the northeastern North America region," *Amer. Fisheries Soc. Symp.*, vol. 41, pp. 183–200, 2005.

[10] E. Vahtmäe, B. Paavel, and T. Kutser, "How much benthic information can be retrieved with hyperspectral sensor from the optically complex coastal waters?," *J. Appl. Remote Sens.*, vol. 14, no. 1, Jan. 2020, Art. no. 0165004, doi: 10.1117/1.JRS.14.016504.

[11] J. T. O. Kirk, *Light and Photosynthesis in Aquatic Ecosystems*. Cambridge, U.K.: Cambridge Univ. Press, 1994.

[12] R. K. Singh and P. Shanmugam, "A novel method for estimation of aerosol radiance and its extrapolation in the atmospheric correction of satellite data over optically complex oceanic waters," *Remote Sens. Environ.*, vol. 142, pp. 188–206, Féb. 2014, doi: 10.1016/j.rse.2013.12.001.

[13] C. D. Mobley, "A numerical-model for the computation of radiance distributions in natural-waters with wind-roughened surfaces," *Limnol. Oceanography*, vol. 34, no. 8, pp. 1473–1483, 1989.

[14] Z. P. Lee, K. L. Carder, C. D. Mobley, R. G. Steward, and J. S. Patch, "Hyperspectral remote sensing for shallow waters. I. A semianalytical model," *Appl. Opt.*, vol. 37, no. 27, pp. 6329–6338, 1998, doi: 10.1364/ao.37.006329.

[15] A. G. Dekker *et al.*, "Intercomparison of shallow water bathymetry, hydro-optics, and benthos mapping techniques in Australian and Caribbean coastal environments," *Limnol. Oceanography Methods*, vol. 9, pp. 396–425, 2011, doi: 10.4319/lom.2011.9.396.

[16] C. D. Mobley *et al.*, "Interpretation of hyperspectral remote-sensing imagery by spectrum matching and look-up tables," *Appl. Opt.*, vol. 44, no. 17, pp. 3576–3592, 2005, doi: 10.1364/AO.44.003576.

[17] Z. Lee, K. L. Carder, C. D. Mobley, R. G. Steward, and J. S. Patch, "Hyperspectral remote sensing for shallow waters: 2. Deriving bottom depths and water properties by optimization," *Appl. Opt.*, vol. 38, no. 18, pp. 3831–3843, 1999.

[18] H. M. Dierssen, R. C. Zimmerman, R. A. Leathers, T. V. Downes, and C. O. Davis, "Ocean color remote sensing of seagrass and bathymetry in the Bahamas banks by high-resolution airborne imagery," *Limnol. Oceanography*, vol. 48, no. 1 II, pp. 444–455, Jan. 2003, doi: 10.4319/lo.2003.48.1_part_2.0444.

[19] S. Andréfouët, C. Payri, E. J. Hochberg, C. Hu, M. J. Atkinson, and . E. Muller-Karger, "Use of *in situ* and airborne reflectance for scaling-up spectral discrimination of coral reef macroalgae from species to communities," *Marine Ecol. Prog. Ser.*, vol. 283, pp. 161–177, Nov. 2004, doi: 10.3354/meps283161.

[20] S. Phinn, C. Roelfsema, A. Dekker, V. Brando, and J. Anstee, "Mapping seagrass species, cover and biomass in shallow waters: An assessment of satellite multi-spectral and airborne hyper-spectral imaging systems in Moreton bay (Australia)," *Remote Sens. Environ.*, vol. 112, no. 8, pp. 3413–3425, 2008, doi: 10.1016/j.rse.2007.09.017.

[21] R. Pu, S. Bell, C. Meyer, L. Baggett, and Y. Zhao, "Mapping and assessing seagrass along the western coast of Florida using landsat TM and EO-1 ALI/Hyperion imagery," *Estuarine Coastal Shelf Sci.*, vol. 115, pp. 234–245, Dec. 2012, doi: 10.1016/j.ecss.2012.09.006.

[22] V. J. Hill, R. C. Zimmerman, W. P. Bissett, H. Dierssen, and D. D. R. Kohler, "Evaluating light availability, seagrass biomass, and productivity using hyperspectral airborne remote sensing in Saint Joseph's Bay, Florida," *Estuaries Coasts*, vol. 37, no. 6, pp. 1467–1489, Oct. 2014, doi: 10.1007/s12237-013-9764-3.

[23] C. M. Duarte, "Reviews and syntheses: Hidden forests, the role of vegetated coastal habitats in the ocean carbon budget," *Biogeosciences*, vol. 14, no. 2, pp. 301–310, 2017, doi: 10.5194/bg-14-301-2017.

[24] M. Lesser and C. Mobley, "Bathymetry, water optical properties, and benthic classification of coral reefs using hyperspectral remote sensing imagery," *Coral Reefs*, vol. 26, no. 4, pp. 819–829, 2007.

[25] H. M. Dierssen, R. C. Zimmerman, L. A. Drake, and D. Burdige, "Benthic ecology from space: Optics and net primary production in seagrass and benthic algae across the great Bahama Bank," *Marine Ecol. Prog. Ser.*, vol. 411, pp. 1–15, 2010.

[26] R. Loizzo *et al.*, "Prisma: The Italian hyperspectral mission," in *Proc. IEEE Int. Geosci. Remote Sens. Symp.*, 2018, pp. 175–178175-178, doi: 10.1109/IGARSS.2018.8518512.

[27] M. Rast and T. H. Painter, "Earth observation imaging spectroscopy for terrestrial systems: An overview of its history, techniques, and applications of its missions," *Surveys Geophys.*, vol. 40, no. 3, pp. 303–331, 2019, doi: 10.1007/s10712-019-09517-z.

[28] J. Chishom *et al.*, "A century of warfare shoots holes in anti-Caulerpa campaign," *Nat. Precedings*, 2007, doi: 10.1038/npre.2007.1240.

[29] J. M. Jaubert, J. R. M. Chisholm, A. Minghelli-Roman, M. Marchioretti, J. H. Morrow, and H. T. Ripley, "Re-evaluation of the extent of caulerpa taxifolia development in the northern Mediterranean using airborne spectrographic sensing," *Marine Ecol. Prog. Ser.*, vol. 263, pp. 75–82, 2003, doi: 10.3354/meps263075.

[30] A. Blanfuné *et al.*, "The CARLIT method for the assessment of the ecological quality of European Mediterranean waters: Relevance, robustness and possible improvements," *Ecological Indicators*, vol. 72, pp. 249–259, 2017, doi: 10.1016/j.ecolind.2016.07.049.

[31] C. H. Köhler, "Airborne imaging spectrometer hyspex," *J. Large-Scale Res. Facilities*, vol. 2, pp. 1–6, Nov. 2016, doi: 10.17815/jlsrf-2-151.

[32] R. Richter and D. Schläpfer, "Atmospheric/topographic correction for satellite imagery (ATCOR-2/3 user guide, version 8.3. 1, February 2014)," ReSe Appl. Schläpfer Langeggweg, vol. 3, 2013.

[33] J. D. Hedley, A. R. Harborne, and P. J. Mumby, "Simple and robust removal of sun glint for mapping shallow-water benthos," *Int. J. Remote Sens.*, vol. 26, no. 10, pp. 2107–2112, 2005, doi: 10.1080/01431160500034086.

[34] L. Louvart and C. Grateau, "The Litto3D project," in *Proc. Eur. Oceans*, 2005, vol. 2, pp. 1244–1251, doi: 10.1109/OCEANSE.2005.1513237.

[35] V. Rey *et al.*, "On the use of long-term observation of water level and temperature along the shore for a better understanding of the dynamics: Example of Toulon area, France," *Ocean Dyn.*, vol. 70, pp. 913–933, May 2020, doi: 10.1007/s10236-020-01363-7.

[36] V. E. Brando, J. M. Anstee, M. Wettle, A. G. Dekker, S. R. Phinn, and C. Roelfsema, "A physics based retrieval and quality assessment of bathymetry from suboptimal hyperspectral data," *Remote Sens. Environ.*, vol. 113, no. 4, pp. 755–770, 2009.

[37] Z. Lee, B. Lubac, J. Werdell, and R. Armone, "An update of the quasi-analytical algorithm (QAA_v5)," *Int. Ocean Color Group Softw. Rep.*, pp. 1–9, 2009.

[38] A. Berk *et al.*, *MODTRAN4 User's Manual*, Air Force Res. Lab., Hanscom AFB, MA, USA, 1999.

[39] S. Michel, M.-J. Lefevre-Fonollosa, and S. Hosford, "HYPXIM–a hyperspectral satellite defined for science, security and defence users" *PAN*, vol. 400, no. 800, p. 400, 2011.

[40] R. L. Lucke *et al.*, "Hyperspectral imager for the coastal ocean: Instrument description and first images," *Appl. Opt.*, vol. 50, no. 11, pp. 1501–1516, 2011, doi: 10.1364/ao.50.001501.

[41] D. Cerra, J. Bieniarz, R. Müller, T. Storch, and P. Reinartz, "Restoration of simulated EnMAP data through sparse spectral unmixing," *Remote Sens*, vol. 7, no. 10, pp. 13190–13207, Oct. 2015.

[42] A. G. Dekker, N. Pinnel, P. Gege, X. Briottet, and A. Court, *Feasibility Study for an Aquatic Ecosystem Earth Observing System Version 1.2*, Feasibility Study for an Aquatic Ecosystem Earth Observing System, CEOS, 2018.

[43] L. Gross, S. Thiria, R. Frouin, and B. G. Mitchell, "Artificial neural networks for modeling the transfer function between marine reflectance and phytoplankton pigment concentration," *J. Geophys. Res. Oceans*, vol. 105, pp. 3483–3495, 2000.

[44] C. J. Legleiter and R. L. Fosness, "Defining the limits of spectrally based bathymetric mapping on a large river," *Remote Sens.*, vol. 11, no. 6, 2019, Art. no. 665.

[45] E. M. Louchard, R. P. Reid, F. C. Stephens, C. O. Davis, R. A. Leathers, and D. T. Valerie, "Optical remote sensing of benthic habitats and bathymetry in coastal environments at lee stocking island, Bahamas: A comparative spectral classification approach," *Limnol. Oceanography*, vol. 48, no. 1, pp. 511–521, 2003.

[46] P. Villa, M. Bresciani, R. Bolpagni, M. Pinardi, and C. Giardino, "A rule-based approach for mapping macrophyte communities using multitemporal aquatic vegetation indices," *Remote Sens. Environ.*, vol. 171, pp. 218–233, 2015.

[47] J. Kotta, K. Remm, E. Vahtmäe, T. Kutser, and H. Orav-Kotta, "In-air spectral signatures of the baltic sea macrophytes and their statistical separability," *J. Appl. Remote Sens.*, vol. 8, no. 1, 2014, Art. no. 083634.

[48] E. Vahtmäe, B. Paavel, and T. Kutser, "How much benthic information can be retrieved with hyperspectral sensor from the optically complex coastal waters?," *J. Appl. Remote Sens.*, vol. 14, no. 1, 2020, Art. no. 016504.